

Selected Paper

Effects of Electrolytes on the Redox Potential and the Rate of the CO Dissociation Reaction of Trinuclear Ruthenium Monocarbonyl Complexes Self-Assembled on an Au(111) Electrode Surface

Takayuki Michi,[1] Masaaki Abe,*[2] Junzo Matsuno,[1] Kohei Uosaki,*[1] and Yoichi Sasaki*[1,†]

[1]Division of Chemistry, Graduate School of Science, Hokkaido University, Kita-ku, Sapporo 060-0810

[2]Department of Applied Chemistry, Graduate School of Engineering, Kyushu University, Nishi-ku, Fukuoka 819-0395

Received December 11, 2006; E-mail: ysasaki@sci.hokudai.ac.jp

Densely packed redox-active self-assembled monolayers (SAMs) of monocarbonyl triruthenium complexes [Ru_3-(μ_3-O)(μ-CH_3COO)$_6$(CO)(mpy)(C10PY)] (**1**) (mpy, 4-methylpyridine; C10PY, {(NC_5H_4)CH_2NHC(O)(CH_2)$_{10}$S–}$_2$), [Ru_3(μ_3-O)(μ-CH_3COO)$_6$(CO)(μ-C10PY)] (**2**), and [{Ru_3(μ_3-O)(μ-CH_3COO)$_6$(CO)(mpy)}$_2$(μ-C10PY)] (**3**) have been constructed on an Au(111) electrode surface. They were characterized by infrared reflection absorption spectroscopy (IRRAS), spectroscopic ellipsometry, and contact angle measurement as well as cyclic voltammetry. Redox potential of the SAMs of **1** at the interface of aqueous electrolyte solutions shifted negatively as the concentration of $HClO_4$ increased from 0.01 to 1.0 mol dm^{-3} with the slope of 0.059 V/decade and as the electrolyte was changed from H_2SO_4 (0.79 V vs. Ag|AgCl) to HNO_3 (0.69 V) and $HClO_4$ (0.59 V) at a fixed concentration of 0.1 mol dm^{-3}. No significant difference in the redox potential was observed between the acid and its sodium salt. The effect is explained, as previously reported for the ferrocenylalkanethiol and non-carbonyl triruthenium SAMs, in terms of the effective ion pair formation in the order $ClO_4^- > NO_3^- > SO_4^{2-}$. The rate of the CO dissociation reaction of the complex in the SAMs (complete within a few minutes at room temperature) that occurs in the oxidation state of $Ru_3^{III,III,III}$ was not very sensitive to the applied electrode potential (0.6–0.8 V), but increased by ca. 2.5 times as the concentration of $HClO_4$ (0.01–1.0 mol dm^{-3}) was lowered, and by ca. one-order of magnitude as the electrolyte anions was changed from ClO_4^- to SO_4^{2-} and NO_3^-.

Construction of molecular-based thin films on solid surfaces is among the most important approaches in modern nanometer-scale science and technology.[1] Transition-metal complexes, especially metal cluster complexes that have versatile physical and chemical properties, are eminent building blocks for such molecular films.[2–4] In that context, oxo-centered triruthenium complexes of the type [Ru_3(μ_3-O)(μ-CH_3COO)$_6$(L)$_3$]$^{n+}$ (L, monodentate ligand) are attractive because they show reversible multi-step redox functions ($Ru_3^{II,II,III}$/$Ru_3^{II,III,III}$/$Ru_3^{III,III,III}$/$Ru_3^{III,III,IV}$/$Ru_3^{III,IV,IV}$) and because synthetic methods are available for modifying three terminal coordination sites (coordinated by L) to control the electronic properties and to introduce functional groups into the trinuclear core.[5–16] It is also noted that the trinuclear core Ru_3(μ_3-O) is a π-conjugated system based on dπ(Ru)–pπ(O) interaction.[5–7,9,16–18] We have recently prepared self-assembled monolayers (SAMs) of the triruthenium complexes on gold electrode surface by using *S*-anchored pyridyl ligands that were introduced onto one of the terminal coordination sites of the core.[19–27]

Among μ_3-oxo-triruthenium complexes, the mono-carbonyl derivatives [Ru_3(μ_3-O)(μ-CH_3COO)$_6$(CO)(L)$_2$], which are isolated in the $Ru_3^{II,III,III}$ oxidation state, are particularly interesting in their characteristic electronic state and reactivities.[16,28–30] While in the non-carbonyl $Ru_3^{II,III,III}$ complexes, the oxidation state is delocalized over three Ru centers, the mono-carbonyl complexes are in a charge-localized state with Ru^{II} ion at the Ru–CO center. This is because of the strong back-bonding character of CO ligand.[16,28–30] On oxidation to $Ru_3^{III,III,III}$ state, the CO ligand dissociates from the core. By introducing the carbonyl complex onto the gold electrode surface, CO dissociation is observed at the interface of the Ru_3-complex-modified electrode and electrolyte solution.[20,22–24,26,27] The dissociation occurs within minutes after electrochemical oxidation to the $Ru_3^{III,III,III}$ state. The reaction has been followed by CV and IR and provides a unique opportunity to study kinetics of ligand-substitution reactions of surface-confined molecules.[22–27] The original CO coordination site is occupied by a solvent molecule, but the CO complex is regenerated when the electrode is soaked in CO saturated solution and the trinuclear core in the $Ru_3^{II,III,III}$ oxidation state.[26] It has been shown that the CO dissociation and coordination reactions fit a first-order rate law. It has also been observed that NO complex can form after the CO dissociation at the $Ru_3^{III,III,III}$ state.[24] Thus, in the $Ru_3^{III,III,III}$ oxidation state, NO coordination is favored over CO. CO dissociation is also known to be initiated by photoirradiation of the $Ru_3^{II,III,III}$ state.[13,25,31–33]

The solvent molecule that replaces the CO ligand is easily substituted by another ligand and thus can be used for further reaction. By using a bridging ligand, such as 4,4′-bipyridine, a bilayer of the triruthenium complexes is formed. By repeating

† Present address: Catalysis Research Center, Hokkaido University, Kita-ku, Sapporo 001-0021

Published on the web July 11, 2007; doi:10.1246/bcsj.80.1368

the same procedure, namely, CO dissociation and coordination of the triruthenium CO complex through the bridging ligand, a pentalayered structure of the triruthenium linear chains has been constructed.[23] All of these studies show that the monocarbonyl triruthenium complexes play significant roles in the development and construction of well-designed functional surfaces based on the triruthenium molecular units.

It is known that the redox potentials of the surface-confined molecules on gold in contact with an electrolyte solution are significantly affected by the type of electrolytes in the solution. Initial studies have been carried out extensively for SAMs of ferrocenylalkanethiols on gold surface.[34–37] While the oxidation wave of the ferrocenyl moiety in 0.2 mol dm^{-3} aqueous $NaClO_4$ solution is fairly sharp and reversible, those in 0.2 mol dm^{-3} aqueous KNO_3 and Na_2SO_4 solutions appear at more positive potentials by ca. 200 mV with considerable broadening. The difference is interpreted in terms of the different stability of the ion-pair between the one-electron-oxidized ferrocenyl moiety (total charge increases from 0 to +1) and the anions; ClO_4^- forms more stable ion-pairs. A similar anion dependence has been observed for the surface-confined non-carbonyl triruthenium complex $[Ru_3(\mu_3\text{-O})(\mu\text{-CH}_3\text{COO})_6(\text{mpy})_2(\text{C10PY})]$ (mpy = 4-methylpyridine, C10PY = $\{(NC_5H_4)CH_2NHC(O)(CH_2)_{10}S-\}_2$), where the total charge also increases from 0 to +1.[21] The difference in the redox potentials is smaller (ca. 110 mV) but with the similar trend as the ferrocenyl derivatives.[21] It is obvious that the electrolytes in solution affect the redox and related properties of the surface-confined molecules. The purpose of this work was first to study the influence of electrolyte solutions on the redox potential of monocarbonyl triruthenium complex that is fixed on the gold surface. Factors, such as the type of anions, pH, and electrolyte concentrations, were considered. Second, these effects were examined on the rate of CO dissociation. The CO dissociation reaction provides a unique opportunity to study quantitatively the ligand substitution reactions of surface-confined molecular unit in terms of these various environmental factors and also of electrode potentials.

For the preparation of SAMs, Ru_3–CO complexes that have an *S*-anchored pyridyl ligand were designed. In addition to the previously reported CO complex $[Ru_3(\mu_3\text{-O})(\mu\text{-CH}_3\text{COO})_6(\text{CO})(\text{mpy})(\text{C10PY})]$ (**1**),[20–22] two new derivatives $[Ru_3(\mu_3\text{-O})(\mu\text{-CH}_3\text{COO})_6(\text{CO})(\mu\text{-C10PY})]$ (**2**), and $[\{Ru_3(\mu_3\text{-O})(\mu\text{-CH}_3\text{COO})_6(\text{CO})(\text{mpy})\}_2(\mu\text{-C10PY})]$ (**3**) were isolated in this study (Fig. 1). The redox and the CO dissociation reactions that were studied here are schematically illustrated in Fig. 2.

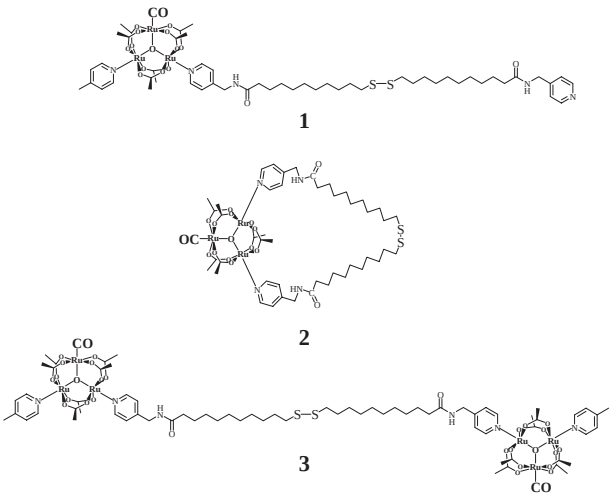

Fig. 1. Schematic structures of complexes **1**, **2**, and **3**.

Experimental

Materials. Reagents and solvents were of commercially available reagent-grade quality unless otherwise stated. The ruthenium salt $RuCl_3 \cdot 3H_2O$ was purchased from Shiga Kikinzoku Co. Silica gel used for column chromatography was Wako gel C-300HG from Wako Chemicals. Water used for the electrolyte solutions was carefully purified by using a Milli-Q water purification system (Simpli Lab, Millipore). The ligand C10PY and complex **1** were prepared according to the methods reported previously.[21,22]

Synthesis of $[Ru_3(\mu_3\text{-O})(\mu\text{-CH}_3\text{COO})_6(\text{CO})(\mu\text{-C10PY})]$ (2) and $[\{Ru_3(\mu_3\text{-O})(\mu\text{-CH}_3\text{COO})_6(\text{CO})(\text{mpy})\}_2(\mu\text{-C10PY})]$ (3). A mixture of complex $[Ru_3(\mu_3\text{-O})(\mu\text{-CH}_3\text{COO})_6(\text{CO})(\text{mpy})(\text{thf})]$ (thf, tetrahydrofuran)[22] (282 mg, 0.33 mmol) and C10PY[21] (861 mg, 1.40 mmol) was dissolved in argon-purged methanol/dichloromethane (60 cm^3, 1:2 v/v). The solution was stirred for 40 h at room temperature under argon. The resultant crude solid was dissolved in 2% methanol/dichloromethane, and the solution was passed through silica-gel column (ϕ2.7 cm × 21 cm). The band on the top of the column was eluted with methanol/dichloromethane with the methanol content increasing gradually from 2 to 6%. A total of seven bands (all deep blue in color) appeared on the column. The solvent was removed from the eluents under a reduced pressure to leave deep blue solid for each band. ^{1}H NMR spectra revealed that the solid samples from the 6th, 4th, and 3rd bands contain complexes **1**, **2**, and **3**, respectively. These solids were recrystallized from THF/*n*-pentane, collected by filtration, washed with *n*-pentane and dried under vacuum. Yields, **1**: 36 mg (7.8%); **2**: 16 mg (3.7%); **3**: 15 mg (2.1%). Complex **2**: Anal. Calcd for $C_{47}H_{72}N_4O_{16}Ru_3S_2$: C, 42.88; H, 5.51; N, 4.26%. Found: C, 42.64; H, 5.63; N, 4.21%. Selected IR data (cm^{-1}, KBr pellet): 2928 w ($\nu_{as}(CH_2)$), 2856 vw ($\nu_s(CH_2)$), 1943 vs (ν(CO, terminal)), 1654 m (ν(CO, C10PY)), 1608 vs (ν_{as}(COO)), 1574 m (ν_{as}(COO)), 1420 vs (ν_s(COO)). FAB-MS (NBA as a matrix): $m/z = 1316$ [M]$^+$. ^{1}H NMR ($CDCl_3$, 20 °C, vs. TMS): δ 9.00 (4H, d, py α-H), 7.92 (4H, d, py β-H), 6.13 (2H, br t, py–CH_2–N*H*–CO–), 4.95 (4H, d, py–C*H*$_2$–NH–), 2.63 (4H, t, –CH_2–SS–CH_2–), 2.38 (4H, t, –CH_2–CO–), 2.08 (12H, s, μ-acetato CH_3), 1.82 (6H, s, μ-acetato CH_3), 1.64–1.51 (16H, br, m, –CH_2–). UV–vis (acetonitrile): λ_{max}/nm (ε/mol dm^{-3} cm^{-1}): 583 (6100), 388 (3300), 329 (8300), 282 (sh, 13400), 228 (sh, 33700). Complex **3**: Anal. Calcd for $C_{72}H_{104}N_6O_{30}Ru_6S_2$: C, 39.23; H, 4.76; N, 3.81%. Found: C, 39.72; H, 5.02; N, 3.56%. Selected IR data (cm^{-1}, KBr pellet): 2928 w ($\nu_{as}(CH_2)$), 2856 vw ($\nu_s(CH_2)$), 1944 vs (ν(CO, terminal)), 1654 m (ν(CO, C10PY)), 1606 vs (ν_{as}(COO)), 1571 m (ν_{as}(COO)), 1420 vs (ν_s(COO)). FAB-MS (NBA as a matrix): $m/z = 2208$ [M]$^+$. ^{1}H NMR ($CDCl_3$, 20 °C, vs. TMS): δ 9.03 (4H, d, mpy α-H), 8.98 (4H, d, py α-H), 7.93 (4H, d, py β-H), 7.85 (4H, d, mpy β-H), 6.32 (2H, br t, py–CH_2–N*H*–CO–), 4.94 (4H, d, py–C*H*$_2$–NH–), 2.87 (6H, s, mpy CH_3), 2.67 (4H, t, –CH_2–SS–CH_2–), 2.37 (4H, t, –CH_2–CO–), 2.08 (12H, s, μ-acetato CH_3), 2.07 (12H, s, μ-acetato CH_3), 1.80 (12H, s, μ-acetato CH_3), 1.64–1.58 (16H, br m, –CH_2–). UV–vis (acetonitrile): λ_{max}/nm (ε/mol dm^{-3} cm^{-1}): 583 (9800), 389 (4700), 329 (12800), 280 (sh, 22000), 228 (sh, 47500).

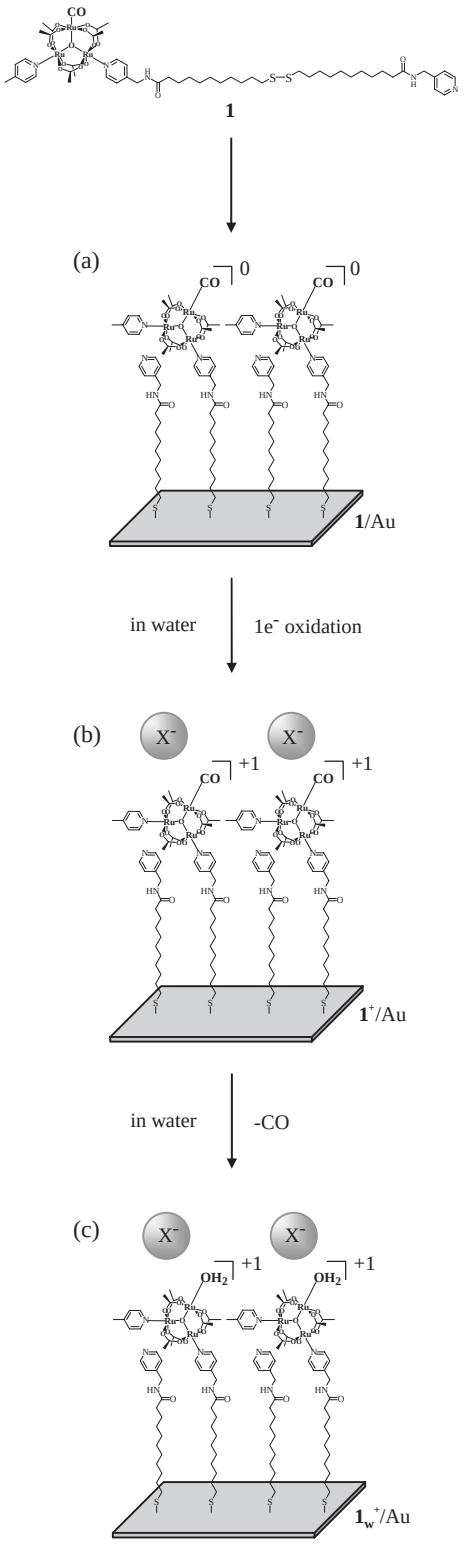

Fig. 2. A schematic representation of monolayer formation of **1** on a gold electrode surface (**1**/Au) and its oxidation ($\mathbf{1}^+$/Au) followed by CO dissociation ($\mathbf{1_w}^+$/Au).

Physical Measurements. Infrared spectra were recorded on a JASCO FT-IR 660 infrared spectrometer using KBr disks. UV–vis spectra were obtained with a Hitachi U-3410 spectrophotometer. ^{1}H NMR spectra were recorded on a JEOL JNM-EX 270 NMR spectrometer at 270.15 MHz. All chemical shifts are reported as δ values downfield from an internal standard of tetramethylsilane (TMS) in $CDCl_3$. Fast-atom bombardment (FAB) mass spectra were recorded on a JEOL JMS-HX110 mass spectrometer in the positive-ion mode using nitrobenzyl alcohol (NBA) as a matrix. FAB mass spectrometry and elemental analysis were performed at the Center for Instrumental Analysis, Hokkaido University.

Preparation of Au(111) Substrates and Self-Assembled Monolayers. A single-crystal Au(111) electrode was prepared at the end of an Au wire (99.99%; 0.8 mm in diameter).[38,39] The Au(111) surface was cleaned before SAM fabrication by flame annealing, followed by quenching in H_2-saturated water. The SAMs of **1**, **2**, and **3** (**1**/Au, **2**/Au, and **3**/Au, respectively) were prepared by immersing the clean Au(111) electrode into a freshly prepared ethanol solution of **1** (10 μmol dm^{-3}), **2** (50 μmol dm^{-3}), and **3** (10 μmol dm^{-3}), respectively, for 24 h.[22] The SAMs-modified Au bead was thoroughly rinsed with ethanol and ultra-pure water, and then transferred to a home-made electrochemical cell with a drop of water to protect the surface against contamination.

Fourier-Transform Infrared Reflection–Absorption Spectroscopy (FT-IRRAS). FT-IR reflection absorption spectra of the SAMs (**1**/Au, $\mathbf{1}^+$/Au ($\mathbf{1}^+$ is the mono-carbonyl complex in the $Ru_3^{III,III,III}$ oxidation state), **2**/Au, and **3**/Au) were recorded at 298 K in dry air on a Bio-Rad FTS-60A/896 spectrometer equipped with a MCT detector and a Harrick grazing angle reflection accessory.[40] Samples for FT-IR reflection absorption measurement were prepared on an evaporated Au substrate (thickness, ≈200 nm) developed on a Ti-coated (≈20 nm) glass plate.

Ellipsometry. Ellipsometry was measured for **1**/Au, $\mathbf{1_w}^+$/Au ($\mathbf{1_w}^+$ is the reaction product of the CO dissociation at the $Ru_3^{III,III,III}$ oxidation state), **2**/Au, and **3**/Au with a SOPRA GESP-5 spectrometer using a 30-W Xe lamp as a light source. The incident angle was set at 75°. The Ψ and Δ values were measured between 300 and 800 nm with a step of 10 nm. Simulation curves were obtained by using a software provided by the manufacturer (SOPRA, WinElli) as follows.[41–43] The complex dielectric functions for the gold surface, $\varepsilon_{Au}(\nu)$, was determined using a bare gold substrate. First, the dielectric functions for the CO-terminated monolayers, $\varepsilon_{CO}(\nu)$, was assumed, reflected on UV–vis absorption spectra in the 300–800 nm range in solution. Next, the thickness of the CO-terminated monolayer was determined using a 3-layer model, air(ε^0)/CO-terminated monolayer($\varepsilon_{CO}(\nu)$, d_{CO})/Au substrate($\varepsilon_{Au}(\nu)$), by the fitting of the calculated $\varepsilon_{CO}(\nu)$ from observed Ψ and Δ values to the model dielectric function based on the dispersion laws.

Contact Angle Measurements. Contact angle of the gold surface modified with **1**/Au, **2**/Au, and **3**/Au were measured by putting a Milli-Q water droplet (11 mg) on the SAMs-modified gold surface and recording the image of the interface with an optical microscope (Intel Play QX3 with magni cation 60). The contact angles were estimated from the recorded digital images of the water droplet on the gold surface. Contact angles for each condition were measured and averaged at least at three different positions on the sample.[44]

Electrochemistry. Cyclic voltammetry of **1**/Au, **2**/Au, and **3**/Au was performed by using Hokuto Denko HZ-3000 electrochemical systems. Pt coil and Ag|AgCl (0.3 mol dm^{-3} NaCl) electrodes were used as counter and reference electrodes, respectively. The measurements were conducted at room temperature. Aqueous solutions containing an appropriate amount of supporting electrolyte were deaerated by passing argon gas for 30 min prior to the measurements. The real surface area of the Au(111) electrode was determined on the basis of charge for the reduction of the gold

Table 1. IR Bands of ν(CO), ν_{as}(COO), and ν_s(COO) of **1**, **1**/Au, $\mathbf{1}^+$/Au, **2**, **2**/Au, **3**, and **3**/Au

Complex	Ru^{III}–ν(CO) /cm^{-1}	Ru^{II}–ν(CO) /cm^{-1}	ν_{as}(COO) /cm^{-1}	ν_s(COO) /cm^{-1}	ν(N–CO) /cm^{-1}	Method
1	—	1951	1607, 1572	1421	1652	KBr
1/Au[a)]	—	1951	1614, 1578	1432	—	IR-RAS
$\mathbf{1}^+$/Au[b)]	2048	1946	—	1431	—	IR-RAS
2	—	1943	1608, 1574	1420	1654	KBr
2/Au[a)]	—	1946	1613, 1584	1431	—	IR-RAS
3	—	1944	1606, 1571	1420	1654	KBr
3/Au[a)]	—	1954	1616, 1576	1421	—	IR-RAS

a) Measured at rest potential. b) Measured for $\mathbf{1}^+$/Au by taking out the electrode from 0.1 mol dm^{-3} $HClO_4$ after maintaining the potential at +0.80 V for several seconds.

oxide in 0.1 mol dm^{-3} H_2SO_4 aqueous solution.

CO Dissociation Kinetics. A series of cyclic voltammograms (CVs) (Figs. 3 and 4, vide infra) were obtained for a Au(111) electrode (0.038 cm^2)[45] covered with densely packed SAM of **1** (**1**/Au). When the electrode potential was set at +0.80 V vs. Ag|AgCl, the CO complex was immediately oxidized to $Ru_3^{III,III,III}$ ($\mathbf{1}^+$) that underwent CO dissociation at a measurable rate. The reactions were monitored by recording CVs at a certain interval in the potential region between +0.80 and −0.30 V at a scan rate of 0.50 V s^{-1}. Decrease in current intensity of CVs of the initial CO complex and the increase in that of the final solvated complex were observed.[22] After each CV measurement, the potential was set back to +0.80 V to continue the CO dissociation reaction. Potential-holding and the CV measurement were repeated at certain time intervals (several seconds; see the caption of Fig. S1) until the completion of the CO dissociation reaction. The amount of CO-coordinating and CO-free complexes on the electrode surface was calculated from the charge under the redox wave at +0.60 V (assigned as $\mathbf{1}/\mathbf{1}^+$; decreasing in intensity with the electrolysis time) and the one at −0.09 V (assigned as $\mathbf{1_w}/\mathbf{1_w}^+$, where $\mathbf{1_w}$ and $\mathbf{1_w}^+$ denote the aquated species [$Ru_3(\mu_3$-O)(μ-$CH_3COO)_6(H_2O)$(mpy)(C10PY)] and its one-electron-oxidized species, respectively. The wave increased in intensity with time).

Results and Discussion

Synthesis. In order to introduce an anchor group to the Au surface by forming a stable Au–S bond, *S*-containing pyridyl ligand C10PY was introduced into the Ru_3 center. Complex **1** was prepared for this purpose as reported in previous studies.[21,22] Careful column chromatographic separation of the products from the preparation of **1** gave the formation of two additional complexes **2** and **3** (Fig. 1) which have not been reported previously.

Complexes **1**, **2**, and **3** were isolated in the mixed-valence form of $Ru_3^{II,III,III}$, in which the divalent state is localized at the Ru–CO center. ^{1}H NMR spectra (270.05 MHz, $CDCl_3$) of **2** and **3** exhibited expected signal patterns of acetate methyl groups: two singlets in a 1:2 signal intensity {δ 1.82 (6H), 2.08 (12H) vs. TMS} for **2**, and three singlets with equal intensities {δ 1.80 (12H), 2.07 (12H), 2.08 (12H) vs. TMS} for **3**. Infrared spectra of **2** and **3** (KBr pellet) showed a strong absorption peak for ν(CO) (1943 and 1944 cm^{-1}, respectively) together with the asymmetric (1608 and 1574, and 1606 and 1571 cm^{-1}, respectively) and symmetric (1420 cm^{-1} for both complexes) stretches for bridging acetate moieties. Additional bands ascribed to carbonyl moieties in C10PY were observed at 1654 cm^{-1} for both complexes. FAB mass spectra of **2** and **3** exhibited a parent peak at $m/z = 1316$ ($[M]^+$) and 2208 ($[M]^+$), respectively. Electronic absorption spectra of **2** and **3** in acetonitrile displayed two intense absorption bands in the visible region ($\lambda_{max} = 583$ and 329 for both complexes) together with a more intense shoulder in the UV region; overall spectral features matched well with those of known carbonyl-containing $Ru_3^{II,III,III}$ analogues [$Ru_3(\mu_3$-O)(μ-$CH_3COO)_6$-(CO)L_2] (L = H_2O, CH_3OH, and pyridine derivatives).[16,30,46]

Formation and Characterizations of Monolayers on Gold. Formation and characterization of the monolayer of **1** on gold surface (**1**/Au) have been reported previously (Fig. 2).[22] The monolayer **1**/Au is a 1:1 mixture of the triruthenium complex and a pyridyl alkanethiolate. CO complexes **2** and **3** were also immobilized on a Au(111) electrode (**2**/Au and **3**/Au). While complex **3** can provide a single monolayer of the triruthenium complex, complex **2** may give a more firmly immobilized monolayer with a two-leg structure. New monolayers **2**/Au and **3**/Au showed CV behaviors characteristic to surface-immobilized redox-active species (linear relation between the scan rate and the current intensity). Some additional characteristic features were observed by IR-reflection absorption spectroscopy, ellipsometry, and contact angle measurement.

Table 1 summarizes the IR bands of the CO ligand stretching ν(CO), the acetate asymmetric (ν_{as}(COO)) and symmetric stretches (ν_s(COO)), and the CO stretching of the C10PY moiety (ν(N–CO)). The data for **1** and **1**/Au were similar to those reported previously.[21,22] The data for **2** and **3** and their SAMs (**2**/Au and **3**/Au) were similar to the corresponding data of **1** and **1**/Au. The (ν(N–CO)) bands were absent in the spectra for **2**/Au and **3**/Au as in the case of **1**/Au, indicating that the directions of the C=O stretch of **2**/Au and **3**/Au as well as **1**/Au are parallel to the surface of the gold electrode.[26] Ellipsometric measurements gave further information on the monolayer structure. Table 2 shows the monolayer thickness as determined by optical ellipsometry for a series of CO-terminated monolayers. The thickness of **1**/Au, **2**/Au, and **3**/Au were ca. 2.0 nm. Considering that the Ru_3 unit is ca. 1.0 nm in size as estimated from X-ray crystal structures of similar triruthenium complexes [$Ru_3(\mu_3$-O)(μ-$CH_3COO)_6$(CO)(*N*-methylbipyridinium$)_2$]$(ClO_4)_2$ and [{$Ru_3(\mu_3$-O)(μ-$CH_3COO)_6$(CO)-(abco)}$_2$(μ-pyrazine)], the length of SAM chain having the Ru_3 head groups is ca. 3.0 nm.[30,47] Thus, it is concluded that the Ru_3 molecule has an inclination of 45° (θ) to the gold electrode surface (Figure in Table 2). It is interesting that the ellipsometric measurements of $\mathbf{1_w}^+$/Au indicates a perpendicular

orientation of $\mathbf{1}_w^+$ ($\theta = 0°$). Contact angle measurements afford wettability of the SAMs-modified gold surface against water. The observed contact angles are shown in Table 3. Contact angles of **1**/Au, **2**/Au, and **3**/Au were larger than that (40.7°) of the bare Au surface. The increase of contact angle indicates that the surface became more hydrophobic, as expected from the nature of ligand environment of the Ru_3 complex on the surface. The difference among **1** (53.0°) and **2** and **3** (ca. 60.5°) may be due to the presence of free pyridyl group in the case of **1**.

Cyclic Voltammograms of CO-Terminated Monolayers. CVs of **1**, **2**, and **3** in acetonitrile solution and those of **1**/Au, **2**/Au, and **3**/Au at the interface of the aqueous electrolyte solutions were measured, and the electrochemical data are summarized in Table 4. CV for **1**/Au was similar to that reported previously, and no further comments are required.[22] The only redox wave observed in the measurable potential window corresponded to the $Ru_3^{II,III,III}/Ru_3^{III,III,III}$ couple. The redox potentials and peak-to-peak separations of the wave of **2**/Au and **3**/Au were similar to those of **1**/Au. The surface coverage of the monolayers of **3** was practically the same to that of **1** (for both cases, 1.3×10^{-10} mol cm^{-2}), and suggests that the pyridyl–alkanethiol component with small head group in **1**/Au does not appear to affect the coverage of the triruthenium complex. These values are consistent with the theoretical value expected for close-packed monolayers, 1.4×10^{-10} mol cm^{-2}, as discussed previously.[30,47] The coverage of **2**/Au (0.9×10^{-10} mol cm^{-2}) was considerably smaller, however, probably because the two-leg structure may fix the orientation of the complex to cause greater steric hindrance and therefore occupy a wider space.

Table 2. Ellipsometric Thickness of **1**/Au, $\mathbf{1}_w^+$/Au, **2**/Au, and **3**/Au

Complex	Observed/nm	Calculated/nm
1/Au	2.1[a]	2.1–2.4[b] ($\theta = 45°$)
$\mathbf{1}_w^+$/Au	3.2	3.0–3.4[b] ($\theta = 0°$)
2/Au	1.9	
3/Au	2.0	

a) Error, 0.2 nm. b) The range is given based on the calculations by rotating the Ru–N bond of the Ru_3 unit.

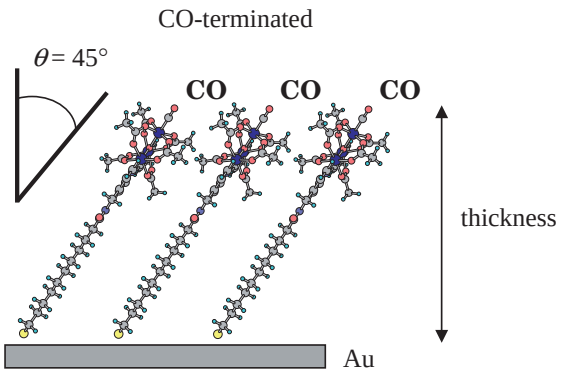

Anion-Dependence of the Redox Potentials. It turned out SAMs containing complexes **1**, **2**, and **3** did not show any significant differences with regard to the redox and other properties. Therefore, the anion dependence on the redox potentials and the subsequent CO dissociation kinetics have been studied only for **1**/Au.

The redox potentials of **1**/Au were measured at the interface of aqueous electrolyte solutions, where the neutral $Ru_3^{II,III,III}$ is oxidized to monocationic $Ru_3^{III,III,III}$ species. The measure-

Table 3. Contact Angles θ_{H2O} of the SAMs Prepared from **1**, **2**, and **3**

Sample	Contact angle θ_{H_2O}
Bare Au surface	40.7° (±2.8°)
1/Au	53.0° (±1.3°)
2/Au	60.5° (±1.9°)
3/Au	60.7° (±1.3°)

Table 4. Electrochemical Data of **1**, **2**, **3**, **1**/Au, **2**/Au, and **3**/Au[a]

Complex	$E_{1/2}$[b]/V vs. Ag|AgCl (ΔE_p[c]/mV) Total charge change ($n/n+1$)[e] (−1/0)	(0/+1)	(+1/+2)	Γ_{Ru3}[d]/mol cm^{-2}	Solution
1	−0.86 (100)	0.65 (80)	1.28 (110)	—	0.1 mol dm^{-3} (n-Bu)$_4$NClO$_4$ in CH$_3$CN
2	−0.86 (210)	0.66 (80)	1.31 (120)	—	0.1 mol dm^{-3} (n-Bu)$_4$NClO$_4$ in CH$_3$CN
3	−0.86 (210)	0.66 (70)	1.30 (120)	—	0.1 mol dm^{-3} (n-Bu)$_4$NClO$_4$ in CH$_3$CN
1/Au	—	0.59 (55)	—	1.3×10^{-10}	0.1 mol dm^{-3} HClO$_4$ in H$_2$O
2/Au	—	0.60 (45)	—	0.9×10^{-10}	0.1 mol dm^{-3} HClO$_4$ in H$_2$O
3/Au	—	0.61 (50)	—	1.3×10^{-10}	0.1 mol dm^{-3} HClO$_4$ in H$_2$O

a) Scan rate of **1**, **2**, and **3** is 0.2 V s^{-1}, and that of **1**/Au, **2**/Au, and **3**/Au is 0.5 V s^{-1}. b) Half-wave potential, $E_{1/2} = (E_{pa} + E_{pc})/2$, where E_{pa} and E_{pc} are anodic and cathodic peak potentials, respectively. c) Peak-to-peak separation, $\Delta E_p = E_{pa} - E_{pc}$. d) Coverage obtained from the cathodic wave. e) n is total charge of $[Ru_3(\mu_3\text{-O})(\mu\text{-CH}_3\text{COO})_6(\text{CO})(\text{mpy})(\text{C10PY})]^n$; $n = -1$ for $[Ru_3^{II,II,III}(\mu_3\text{-O})(\mu\text{-CH}_3\text{COO})_6(\text{CO})(\text{mpy})(\text{C10PY})]^-$ ($\{Ru^{II}\text{–CO}\}Ru_2^{II,III}$), $n = 0$ for $\{Ru^{II}\text{–CO}\}Ru_2^{III,III}$, $n = +1$ for $\{Ru^{III}\text{–CO}\}Ru_2^{III,III}$, and $n = +2$ for $\{Ru^{III}\text{–CO}\}Ru_2^{III,IV}$.

Table 5. $E_{1/2}$ of the $Ru_3^{II,III,III}/Ru_3^{III,III,III}$ Couple of **1**/Au at the Interface of Various Aqueous Electrolyte Solutions

Electrolyte	$E_{1/2}$/V
1 mol dm^{-3} $HClO_4$	0.53
0.1 mol dm^{-3} $HClO_4$	0.59
0.01 mol dm^{-3} $HClO_4$	0.64
0.1 mol dm^{-3} HNO_3	0.69
0.1 mol dm^{-3} H_2SO_4	0.79
0.1 mol dm^{-3} $NaClO_4$	0.60
0.1 mol dm^{-3} $NaNO_3$	0.69
0.1 mol dm^{-3} Na_2SO_4	—[a)]

a) Not observed.

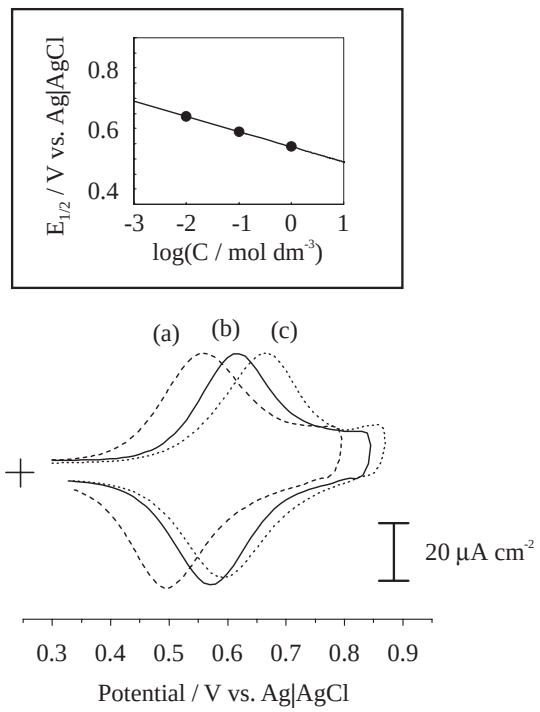

Fig. 3. Lower: Cyclic voltammograms of **1**/Au recorded in aqueous electrolyte solutions of (a) 1 mol dm^{-3} $HClO_4$, (b) 0.1 mol dm^{-3} $HClO_4$, and (c) 0.01 mol dm^{-3} $HClO_4$. Scan rate is 0.5 V s^{-1}. Upper: Dependence of the redox potentials of **1**/Au on $HClO_4$ concentration.

ments were carried out by changing the concentrations of electrolytes, type of anion, and pH of the solutions. Table 5 is a comparison of the redox potential of **1**/Au at the interface of aqueous acidic solutions containing $HClO_4$, HNO_3, and H_2SO_4 and of neutral aqueous media containing their sodium salts, as well as those in different concentrations of $HClO_4$ (0.01, 0.1, and 1 mol dm^{-3}). The redox potential of **1**/Au shifted to negative potentials with an increase in the concentration of $HClO_4$ (Fig. 3). Thus, the positively charged oxidized form is more stabilized at higher concentrations of $HClO_4$. The slope of the plot of the redox potential against the $HClO_4$ concentration was 59 mV per one magnitude change of the concentration. As discussed previously for ferrocenylalkanethiol SAMs,[34–36] the present results are also interpreted in terms of the ion-pair formation between the oxidized species and ClO_4^-.

Table 5 also shows the redox potentials of **1**/Au at the interface of the solution of different electrolytes. Figure 4 shows CVs in ClO_4^-, NO_3^-, and SO_4^{2-} media. A significant positive shift of the redox potential was observed on going from ClO_4^- to NO_3^- and SO_4^{2-} media with considerable broadening[48] of the redox wave. The redox potentials were practically the same between 0.1 mol dm^{-3} $HClO_4$ and $NaClO_4$ media as well as between 0.1 mol dm^{-3} HNO_3 and $NaNO_3$ solutions. Thus, the pH of the solution does not affect the redox potential. The type of anions gave significant effect, however, as noted previously for the SAMs of ferrocenylalkanethiol.[34–36] The order of the positive shift of the redox potentials of **1**/Au at the interface of aqueous 0.1 mol dm^{-3} electrolyte solution was $ClO_4^- < NO_3^- < SO_4^{2-}$. Previous studies on the SAMs of metal complexes on gold reported the following order for the positive shift of the redox potentials: $PF_6^- < ClO_4^- < BF_4^- < NO_3^- < Cl^- < SO_4^{2-} < NH_2SO_3^- < F^-$ for the ferrocenylalkanethiol[33–36] and $PF_6^- < ClO_4^- \approx CF_3SO_3^- < SO_4^{2-} < NO_3^-$ for the non-carbonyl complex $[Ru_3(\mu_3\text{-}O)(\mu\text{-}CH_3COO)_6(mpy)_2(C10PY)]$.[21] Although the difference in the order of SO_4^{2-} and NO_3^- has been noted between the systems, the most significant observation is that ClO_4^- always gives the most negative redox potentials and, therefore, forms the strongest ion-pair with the positively charged oxidized complexes. As discussed previously,[33–35] this is explained by smaller dehydration energy of ClO_4^- resulting in a higher degree of ion-pair formation. Another interesting observation is that the carbonyl triruthenium complex on gold surface is significantly more sensitive to the type of anions as compared to analogous non-carbonyl triruthenium complexes. This may be due to more hydrophobic nature of the carbonyl complex.[49]

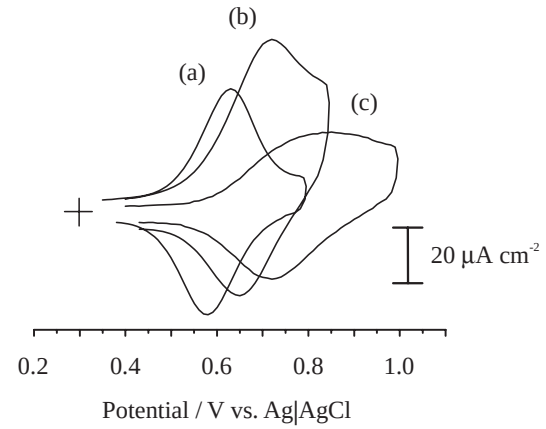

Fig. 4. Cyclic voltammograms of **1**/Au recorded in aqueous electrolyte solutions of (a) 0.1 mol dm^{-3} $HClO_4$, (b) 0.1 mol dm^{-3} HNO_3, and (c) 0.1 mol dm^{-3} H_2SO_4. Scan rate is 0.5 V s^{-1}.

Effects of Electrolytes and Electrode Potential on the Rate of the CO Dissociation Reaction. The CO dissociation reaction takes place in the one-electron oxidized complex $[Ru_3(\mu_3\text{-}O)(\mu\text{-}CH_3COO)_6(CO)(mpy)(C10PY)]^+$. When the electrode potential was set to the potential where the complex is in the oxidized form, entire trinuclear species on the surface $[Ru_3(\mu_3\text{-}O)(\mu\text{-}CH_3COO)_6(CO)(mpy)(C10PY)]$ ($\{Ru^{II}\text{–}CO\}\text{-}Ru_2^{III,III}$) in **1**/Au are instantaneously oxidized to $\{Ru^{III}\text{–}CO\}\text{-}Ru_2^{III,III}$ (**1**$^+$/Au) (Fig. 2). Then, the CO dissociation reaction occurs at a measurable rate (within few minutes at room tem-

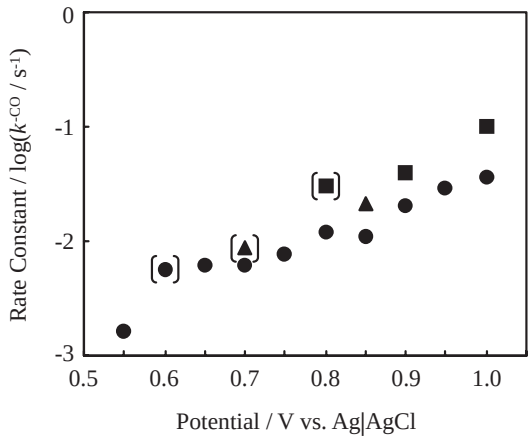

Fig. 5. The relationship between electrode potentials and rate constants of the CO dissociation reaction of $\mathbf{1}^+$/Au in 0.1 mol dm^{-3} $HClO_4$ (●), 0.1 mol dm^{-3} HNO_3 (▲), and 0.1 mol dm^{-3} H_2SO_4 (■). The data points in parentheses are taken at $E_{1/2}$.

perature) at the interface of the aqueous electrolyte solution.[22] Rate of the CO dissociation from $\mathbf{1}^+$/Au was monitored by measuring CVs at certain intervals as mentioned in the Experimental Section.

$$[Ru_3(\mu_3\text{-O})(\mu\text{-}CH_3COO)_6(CO)(mpy)(C10PY)]^+ + H_2O \rightarrow [Ru_3(\mu_3\text{-O})(\mu\text{-}CH_3COO)_6(H_2O)(mpy)(C10PY)]^+ + CO. \quad (1)$$

Regardless of the varying electrode potentials and different electrolyte solutions, the CV changes, and therefore the CO dissociation reactions proceeded in the first-order manner (see Fig. S1). It appears that the first-order rate constants (k^{-CO}) evaluated under these conditions were different from each other.

Dependence of the rate constant on the applied potential was studied in 0.1 mol dm^{-3} $HClO_4$ media. Except for the potential at +0.55 V, which is close to the half-wave potential, the major species on the surface should be the oxidized one. The smaller rate constant at +0.55 V may be explained by smaller concentration of the oxidized species (about the half of the total amount of the complex). Figure 5 shows the rate constant vs. electrode potential. It is noteworthy that on increasing the potential, the rate constant initially showed only a slight increase up to +0.75 V and then increased more sharply. Since the initial increase is small, a sharp increase at higher potential should not be caused by the potential change. It is known that further oxidation of $\mathbf{1}^+$ occurs at +1.28 V in acetonitrile containing 0.1 mol dm^{-3} $(n\text{-}Bu)_4NClO_4$.[22] It is possible that the two-electron-oxidized species undergoes the CO dissociation reaction very rapidly as our preliminary experiment shows. Such rapid reaction would influence the rate of CO dissociation, when the potential becomes more positive. Thus, it is concluded that the intrinsic influence of the electrode potential on the rate constant is only marginal.

Table 6 shows k^{-CO} for CO dissociation reaction of $\mathbf{1}^+$/Au at the interface of aqueous solutions containing various electrolytes and different concentration (0.01, 0.1, and 1 mol dm^{-3}) of $HClO_4$. Since k^{-CO} slightly depended on the applied potential, the potential was set to $E_{1/2}$ of each electrolyte solution, where half of the complex is in the oxidized form, and also set to ca. 0.2 V more positive than $E_{1/2}$ (denoted as E_{III}), where the complex is almost entirely in the oxidized form. As expected, the rate in each electrolyte medium was faster at E_{III} than at $E_{1/2}$ by at least two times. Nevertheless, the general trend in k^{-CO} was similar for the two sets (at E_{III} and at $E_{1/2}$) of the data. k^{-CO} depended on the concentration of $HClO_4$ and was larger at lower concentration; k^{-CO} in 0.01 mol dm^{-3} $HClO_4$ was more than two times greater than that in 1 mol dm^{-3} $HClO_4$. This fact indicates that ion-pair formation retards the CO dissociation reaction. The rate constant may depend on the solution pH, since the value in 0.1 mol dm^{-3} $HClO_4$ (or HNO_3) is clearly larger by a few times than that in 0.1 mol dm^{-3} $NaClO_4$ (or $NaNO_3$). The change is small, however, when the large pH change (ca. 7) is considered and is not significant enough for further discussion. With regard to the influence of the type of anions, k^{-CO} showed a large difference; it increased in the order of $ClO_4^- < NO_3^- < SO_4^{2-}$. The trend was observed both in the neutral electrolyte and acidic solutions and indicates that the anion forms strong ion-pair with $\mathbf{1}^+$/Au, retarding the CO dissociation reaction as concluded for the $HClO_4$ concentration dependence. It may be that the CO dissociation reaction is assisted by the solvent water molecules, which are less available when the solvational structure is destroyed by the ion-pair formation.

Table 6. First-Order Rate Constants (k^{-CO}) of the CO Dissociation Reaction of $\mathbf{1}^+$ in $\mathbf{1}^+$/Au at the Interface of Various Aqueous Electrolyte Solutions

Electrolyte	(k^{-CO} at $E_{1/2}$)/s^{-1} ($E_{1/2}$/V[a)])	(k^{-CO} at E_{III})/s^{-1} (E_{III}/V)
1 mol dm^{-3} $HClO_4$	2.9×10^{-3} (0.53)	6.2×10^{-3} (0.80)
0.1 mol dm^{-3} $HClO_4$	5.6×10^{-3} (0.59)	1.2×10^{-2} (0.80)
0.01 mol dm^{-3} $HClO_4$	7.9×10^{-3} (0.64)	1.5×10^{-2} (0.80)
0.1 mol dm^{-3} HNO_3	8.8×10^{-3} (0.69)	2.1×10^{-2} (0.90)
0.1 mol dm^{-3} H_2SO_4	3.0×10^{-2} (0.79)	1.0×10^{-1} (1.00)
0.1 mol dm^{-3} $NaClO_4$	1.3×10^{-2} (0.60)	3.0×10^{-2} (0.80)
0.1 mol dm^{-3} $NaNO_3$	5.7×10^{-2} (0.69)	1.4×10^{-1} (0.90)

a) $E_{1/2}$ is the half-wave potential of the $Ru_3^{II,III,III}/Ru_3^{III,III,III}$ couple.

Finally, it is interesting to note that the CO dissociation reaction was retarded significantly when the electrode in the $\mathbf{1}^+$/Au form was taken out from the electrolyte solution. The Au electrode ($\mathbf{1}^+$/Au) was maintained at a potential of +0.80 V for several seconds in 0.1 mol dm^{-3} $HClO_4$ aqueous solution and was taken out from the solution. The electrode was dried with argon gas, and then FT-IRRAS spectra of the $\{Ru^{III}\text{–}CO\}Ru_2^{III,III}$ monolayer were measured in air. A strong ν(CO) band for the $\{Ru^{III}\text{–}CO\}Ru_2^{III,III}$ state[26,29] was observed after these treatments together with a smaller band for $\{Ru^{II}\text{–}CO\}Ru_2^{III,III}$.[26,29] The latter species partially formed during the

treatments. Thus, it is clear that the Ru^{III}–CO bond is stabilized to some extent when electrode $\mathbf{1}^{+}$/Au was removed from the bulk aqueous electrolyte solution.

Conclusion

Self-assembled mono-carbonyl triruthenium cluster complexes $[Ru_3(\mu_3\text{-}O)(\mu\text{-}CH_3COO)_6(CO)(mpy)(C10PY)]$ (**1**) ($\{Ru^{II}\text{–}CO\}Ru_2^{III,III}$) on the gold surface (**1**/Au) was shown to be useful for the construction of functional nano-scale materials on the solid surface as CO dissociation causes a change in the ligand environment of the triruthenium unit. CO dissociation is initiated by the one-electron oxidation to $Ru_3^{III,III,III}$ state ($\mathbf{1}^{+}$/Au), the potential of which was examined in terms of the influence of the electrolytes used in the aqueous media for the CV measurements. It turned out that the redox potential was strongly influenced by the type of anions: ClO_4^- (+0.59) < NO_3^- (+0.69) < SO_4^{2-} (+0.79 V vs. Ag|AgCl) (0.1 mol dm^{-3}). Strong ion-pair formation with the monopositive oxidized species causes the oxidation to become more favorable. A hydrophobic CO head group would make the influence of ion-pair formation stronger. Rate constant (k^{-CO}) of the CO dissociation that occurs at the interface of the aqueous electrolyte solution in the $Ru_3^{III,III,III}$ state was dependent on the electrolyte and was different by as much as one order of magnitude depending on the type of electrolytes. Ion-pair formation appears to retard the CO dissociation reaction possibly by disturbing a solvent-assisted pathway of the reaction. The CO coordinated $Ru_3^{III,III,III}$ species is stabilized against CO dissociation in the solvent-free $\mathbf{1}^{+}$/Au state.

This work was partly supported by Grant-in-Aids for Scientific Research on Priority Area of "Reaction Control of Dynamic Complexes" (No. 16033201) to YS and "Chemistry of Coordination Space" (No. 18033039) to MA from the Ministry of Education, Culture, Sports, Science and Technology of Japan. The authors are grateful to Professors M. Osawa and S. Ye of the Catalysis Research Center, Hokkaido University, for their assistance in the measurements of contact angle and FT-IR spectroscopy.

Supporting Information

Kinetic analysis of the CO dissociation reaction for **1**/Au. This material is available free of charge on the Web at: http://www.csj.jp/journals/bcsj/.

References

1 *Interfacial Electrochemistry: Theory, Experiment, and Applications*, ed. by A. Wieckowski, Marcel Dekker, New York, **1999**.

2 H. Doron-Mor, A. Hatzor, A. Vaskevich, T. van der Boom-Moav, A. Shanzer, I. Rubinstein, H. Cohen, *Nature* **2000**, *406*, 382.

3 S. Yasutomi, T. Morita, Y. Imanishi, S. Kimura, *Science* **2004**, *304*, 1944.

4 L. F. O. Furtado, A. D. P. Alexiou, L. Goncalves, H. E. Toma, K. Araki, *Angew. Chem., Int. Ed.* **2006**, *45*, 3143.

5 R. D. Cannon, R. P. White, *Prog. Inorg. Chem.* **1988**, *36*, 195.

6 H. E. Toma, K. Araki, A. D. P. Alexiou, S. Nikolaou, S. Dovidauskas, *Coord. Chem. Rev.* **2001**, *219–221*, 187.

7 Y. Sasaki, M. Abe, *Chem. Rec.* **2004**, *4*, 279.

8 J.-K. Chen, L.-Y. Zhang, Z.-N. Chen, L.-B. Gao, M. Abe, Y. Sasaki, *Inorg. Chem.* **2004**, *43*, 1481.

9 T. Hamaguchi, H. Nagino, K. Hoki, H. Kido, T. Yamaguchi, B. K. Breedlove, T. Ito, *Bull. Chem. Soc. Jpn.* **2005**, *78*, 591.

10 R. C. Rocha, M. G. Brown, C. H. Londergan, J. C. Salsman, C. P. Kubiak, A. P. Shreve, *J. Phys. Chem. A* **2005**, *109*, 9006.

11 J.-L. Chen, L.-Y. Zhang, L.-X. Shi, H.-Y. Ye, Z.-N. Chen, *Inorg. Chim. Acta* **2006**, *359*, 1531.

12 H.-Y. Ye, L.-Y. Zhang, J.-L. Chen, Z.-N. Chen, *Chem. Commun.* **2006**, 1971.

13 M. Itou, Y. Araki, O. Ito, H. Kido, *Inorg. Chem.* **2006**, *45*, 6114.

14 G. S. Nunes, A. D. P. Alexiou, K. Araki, A. L. B. Formiga, R. C. Rocha, H. E. Toma, *Eur. J. Inorg. Chem.* **2006**, 1487.

15 S. E. Toma, H. E. Toma, *Electrochem. Commun.* **2006**, *8*, 1628.

16 J. A. Baumann, D. J. Salmon, S. T. Wilson, T. J. Meyer, W. E. Hatfield, *Inorg. Chem.* **1978**, *17*, 3342.

17 Y. Sasaki, A. Tokiwa, T. Ito, *J. Am. Chem. Soc.* **1987**, *109*, 6341.

18 M. Tanaka, N. Kariya, M. Abe, Y. Sasaki, *Bull. Chem. Soc. Jpn.* **2007**, *80*, 192.

19 M. Abe, T. Kondo, K. Uosaki, Y. Sasaki, *J. Electroanal. Chem.* **1999**, *473*, 93.

20 M. Abe, S. Ye, T. Kondo, K. Uosaki, Y. Sasaki, *Electrochemistry* **1999**, *67*, 1162.

21 M. Abe, A. Sato, T. Inomata, T. Kondo, K. Uosaki, Y. Sasaki, *J. Chem. Soc., Dalton Trans.* **2000**, 2693.

22 A. Sato, M. Abe, T. Inomata, T. Kondo, S. Ye, K. Uosaki, Y. Sasaki, *Phys. Chem. Chem. Phys.* **2001**, *3*, 3420.

23 M. Abe, T. Michi, A. Sato, T. Kondo, W. Zhou, S. Ye, K. Uosaki, Y. Sasaki, *Angew. Chem., Int. Ed.* **2003**, *42*, 2912.

24 S. Ye, W. Zhou, M. Abe, T. Nishida, L. Cui, K. Uosaki, M. Osawa, Y. Sasaki, *J. Am. Chem. Soc.* **2004**, *126*, 7434.

25 M. Abe, T. Masuda, T. Kondo, K. Uosaki, Y. Sasaki, *Angew. Chem., Int. Ed.* **2005**, *44*, 416.

26 W. Zhou, S. Ye, M. Abe, T. Nishida, K. Uosaki, M. Osawa, Y. Sasaki, *Chem. Eur. J.* **2005**, *11*, 5040.

27 T. Michi, M. Abe, S. Ye, M. Osawa, T. Kondo, K. Uosaki, Y. Sasaki, ECS Proceedings Volume, Electrode Processes VII, **2005**, p. 116.

28 M. Abe, Y. Sasaki, A. Nagasawa, T. Ito, *Bull. Chem. Soc. Jpn.* **1992**, *65*, 1411.

29 S. Ye, H. Akutagawa, K. Uosaki, Y. Sasaki, *Inorg. Chem.* **1995**, *34*, 4527.

30 M. Abe, Y. Sasaki, Y. Yamada, K. Tsukahara, S. Yano, T. Yamaguchi, M. Tominaga, I. Taniguchi, T. Ito, *Inorg. Chem.* **1996**, *35*, 6724.

31 D. Akashi, H. Kido, M. Abe, Y. Sasaki, T. Ito, *Dalton Trans.* **2004**, 2883.

32 M. Itou, M. Otake, Y. Araki, O. Ito, H. Kido, *Inorg. Chem.* **2005**, *44*, 1580.

33 M. Otake, M. Itou, Y. Araki, O. Ito, H. Kido, *Inorg. Chem.* **2005**, *44*, 8581.

34 K. Uosaki, Y. Sato, H. Kita, *Langmuir* **1991**, *7*, 1510.

35 K. Uosaki, *Electrochemistry* **1999**, *67*, 1105.

36 G. K. Rowe, S. E. Creager, *Langmuir* **1991**, *7*, 2307.

37 G. Valincius, G. Niaura, B. Kazakeviciene, Z. Talaikyte,

M. Kazemekaite, E. Butkus, V. Razumas, *Langmuir* **2004**, *20*, 6631.

38 K. Uosaki, S. Ye, T. Kondo, *J. Phys. Chem.* **1995**, *99*, 14117.

39 T. Kondo, S. Horiuchi, I. Yagi, S. Ye, K. Uosaki, *J. Am. Chem. Soc.* **1999**, *121*, 391.

40 A. Miki, S. Ye, M. Osawa, *Chem. Commun.* **2002**, 1500.

41 K. Uosaki, T. Kondo, M. Okamura, W. Song, *Faraday Discuss.* **2002**, *121*, 373.

42 R. M. A. Azzam, N. M. Bashara, *Ellipsometry and Polarized Light*, North-Holland, Amsterdam, **1977**.

43 J. Shi, B. Hong, A. N. Parikh, R. W. Collins, D. L. Allara, *Chem. Phys. Lett.* **1995**, *246*, 90.

44 S. Ye, G. Li, H. Noda, K. Uosaki, M. Osawa, *Surf. Sci.* **2003**, *529*, 163.

45 The surface area of the Au electrode was determined based on the observed charge in the cyclic voltammogram for the reduction of gold oxide using 0.1 mol dm^{-3} H_2SO_4 solution.

46 J. A. Baumann, S. T. Wilson, D. J. Salmon, P. L. Hood, T. J. Meyer, *J. Am. Chem. Soc.* **1979**, *101*, 2916.

47 T. Yamaguchi, N. Imai, T. Ito, C. P. Kubiak, *Bull. Chem. Soc. Jpn.* **2000**, *73*, 1205.

48 Although the anion dependence of the redox potential is reasonably explained as in the text, the reason for the broadening of the redox wave as the electrolyte anions change from ClO_4^- to NO_3^- and SO_4^{2-} is more difficult to discuss at this stage. The densely packed structure in the monolayer may cause a less smooth transfer of the latter anions during the redox process, since the redox wave of the mixed-monolayer of the triruthenium complex and alkanethiols, where anions can approach the complex more easily, show much lesser extent of the broadening with the change of the electrolyte anions (Michi et al., unpublished).

49 Due to the poor solubility of the neutral monocarbonyl triruthenium ($\{Ru^{II}–CO\}Ru_2^{III,III}$) complexes, comparative studies of the influence of the electrolytes of discrete complexes in solution were not carried out. The redox potentials ($Ru_3^{II,III,III}/Ru_3^{III,III,III}$ couple) of $[Ru_3(\mu_3\text{-}O)(\mu\text{-}CH_3COO)_6(CO)(mbpy^+)_2]^{2+}$ ($mbpy^+$, *N*-methyl-4,4′-bipyridinium ion),[30] which were determined under the corresponding conditions of the **1**/Au showed similar anion dependence but the change was in much narrower range (0.62 (1 mol dm^{-3} $HClO_4$)–0.70 V (0.1 mol dm^{-3} H_2SO_4)). The direct comparison is not feasible because of the different type of charge change (+2/+3).